Hydrogen effects in X30MnCrN16-14 austenitic steel

Einfluss von Wasserstoff in dem austenitischen Stahl X30MnCrN16-14

T. Michler[1, 4], E. Bruder[2], S. Lindner[3]

Chrome-manganese-nitrogen austenitic steels show a technically relevant combination of proprties, i. e. high strength, high ductility, non magnetic and good corrosion resistance at costs being much lower compared to conventional chrome-nickel austenitic stainless steels which are widely used for hydrogen applications. Hydrogen environment embrittlement of steel X30MnCrN16-14 is investigated by slow displacement rate tensile testing in hydrogen atmosphere at 10 MPa and room temperature. Compared to the values in air, the elongation at fracture as well as the reduction of area are severely reduced in the presence of hydrogen. The microstructure is characterized in detail and the deformation modes are previously reported. It is assumed that the inherent planar deformation modes are facilitated by hydrogen resulting in premature failure.

Keywords: Hydrogen embrittlement **/** austenitic manganese nitrogen steel **/** microstructure **/** deformation mechanism **/** tensile testing.

Austenitische Stähle auf Basis Chrom-Mangan-Stickstoff kombinieren eine hohe Festigkeit mit hoher Duktilität, nicht magnetischen Eigenschaften und guter Korrosionsbeständigkeit. Dabei sind die Werkstoffkosten geringer als die konventioneller austenitischer Stähle auf Basis von Chrom und Nickel, welche als Standardwerkstoffe für Wasserstoffanwendungen gelten. Die Neigung zur Wasserstoffversprödung des Stahls X30MnCrN16-14 wird mithilfe von Zugversuchen mit langsamer Abzugsgeschwindigkeit in Wasserstoffatmosphäre bei einem Druck von 10 MPa und Raumtemperatur untersucht. Im Vergleich zu den Werten in Luft sind beim Test in Wasserstoffatmosphäre die Bruchdehnung und die Brucheinschnürung stark reduziert. Das Gefüge des untersuchten Stahls wird detailliert charakterisiert und der Verformungsmechanismus wurde in anderen Publikationen identifiziert. Mit diesen Informationen kann geschlussfolgert werden, dass die inhärenten planaren Versetzungsbewegungen durch den Einfluss von Wasserstoff verstärkt werden, was zu einem frühzeitigen Versagen führt.

Schlüsselwörter: Wasserstoffversprödung **/** austenitischer Mangan-Stickstoff-Stahl **/** Gefüge **/** Verformungsmechanismus **/** Zugversuch

[1] Opel Automobile GmbH, Bahnhofsplatz 1, 65423 Rüsselsheim am Main RUESSELSHEIM, GERMANY

[2] Technische Universität Darmstadt, Materials Science Department, Physical Metallurgy Division, Alarich-Weiß-Straße 2, 64287 Darmstadt DARMSTADT, GERMANY

[3] Outokumpu Nirosta GmbH, Oberschlesienstraße 16, 47807 KREFELD, GERMANY

[4] Fraunhofer-Institut für Werkstoffmechanik IWM

Corresponding author: T. Michler, Opel Automobile GmbH, Bahnhofsplatz 1, 65423 Rüsselsheim am Main RUESSELSHEIM, GERMANY,
E-Mail: thorsten.dr.michler@opel-vauxhall.com

1 Introduction

Typical steels for common high-pressure compressed hydrogen tank components for automotive applications (e.g. bosses, valve bodies, pipes, fittings) are conventional chrome-nickel austenitic stainless steels (SS). However, the low nickel containing grades like AISI/SUS 304 or DIN 1.4301 suffer from hydrogen environment embrittlement under the given conditions. That is, grade AISI/SUS 316 or DIN 1.4435 with a high nickel content is mostly used [1].

Nickel and molybdenum are the cost drivers in stainless steels which makes these grades unattractive for automotive applications. It would be a big cost savings effect if it were possible to replace nickel and molybdenum by a combination of alternative alloying elements, especially manganese and nitrogen, both of which are much more cost effective. A new class of nickel free austenitic stainless steels has been developed recently for a variety of applications [2–8]. In such steels, the austenite is stabilized by a combination of manganese, nitrogen and carbon. These steels show a unique combination of properties, i.e. high strength, high ductility, non magnetic and good corrosion resistance at costs being 25 % to 50 % lower compared to conventional stainless steels. At this cost range such steels become attractive for selected automotive applications. A variety of such steels were tensile tested in high pressure hydrogen atmosphere and all of them showed a severe degradation of tensile ductility which was attributed to the inherent planar deformation mechanisms amplified by hydrogen supporting the hydrogen enhanced localized plasticity (HELP) theory [9, 10]. However, since hydrogen embrittlement of metals is still not completely understood, it is helpful to test new materials to either support or refute existing embrittlement theories. Reports on hydrogen effects in steel X30MnCrN16-14 (grade 1.4678) could not be found in the open literature and the motivation of this work was to study the tensile response of this steel is gaseous hydrogen atmosphere.

2 Experimental details

Steel X30MnCrN16-4 was provided as rolled plate semi-finished product in solution annealed condition. The chemical composition is given in *Table 1*. The microstructure was evaluated by conventional metallography using Lichtenegger-Bloech colour etchant as well as by scanning electron microscopy (scanning electron microscopy), electron back scatter detection (electron back scatter detection) and electron channelling contrast imaging (electron channelling contrast imaging) [11]. High resolution scanning electron microscopy analyses were performed at TU Darmstadt using a FEG-scanning electron microscopy (MIRA3-XMH by TESCAN, Brno, Czech Republic) equipped with a 4-quadrant solid state back scatter electron (BSE) detector (DEBEN Ltd., London, UK) and an electron back scatter detection system (DigiView IV by EDAX, AMETEK Inc., Berwyn, USA). An acceleration voltage of 20 kV was used for electron back scatter detection and electron channelling contrast imaging. The electron back scatter detection analysis was performed with a step size of 150 nm using a confidence index (CI) standardization cleanup routine and excluding all points with a $CI < 0.1$ from the analysis. For electron channelling contrast imaging, grains with a low backscattering coefficient were selected from a low magnification image. The sample was then titled and rotated for each grain to maximize its contrast of lattice defects at high magnifications.

The amount of tetragonal distorted cubic body centered (bct) martensite was measured by magnetic induction using a Feritscope (model MP30E-S by Fischer GmbH, Sindelfingen, Germany).

Tensile tests in 10 MPa hydrogen gas (purity 99.9999 %) at ambient temperature were performed at the Materials Testing Institute University of Stuttgart (Germany) with a test apparatus described in [12]. Reference tests in air at ambient temperature were performed at Opel using an Instron 5855 test machine with a 200 kN load cell.

Table 1. Chemical composition of the heat investigated in this study. All values in [wt %].

Grade	C	Si	Mn	P	S	Cr	Cu	N
X30MnCrN16-14 (1.4678)	0.31	0.39	15.91	0.025	0.002	14.01	0.50	0.33

Cylindrical specimens (diameter 3 mm, gauge length 30 mm) were machined out of a rolled plate semi-finished product and tensile tested as machined. For all tests, the cross head speed was set to 0.1 mm/min. Fractography was performed using a LEO 1455VP scanning electron microscopy (SEM) with a tungsten electrode.

3 Results and discussion

The microstructure in solution treated and not deformed condition was analysed in detail, *Figure 1*. The microstructure was completely austenitic with a significant amount of annealing twin boundaries, as verified by colour etching as well as by electron back scatter detection, Figure 1a–c. The grain size was about 40 μm. As an effect of the rolling process and using Lichtenegger-Bloech etchant, macro segregations of the main alloying elements (i.e. manganese and chrome) appear as wavy (horizontal) features [13], Figure 1a. This etching technique also revealed parallel features inside the grains with a spacing in the order of 100 nm to 500 nm which were not observed by electron back scatter detection, Figure 1b, c. Further analysis using electron channelling contrast imaging revealed features with a similar spacing, which were interpreted as stacking faults, Figure 1d. This might be confirmed by transmission electron microscopy, which was not part of this study. That is, the parallel features observed by optical microscopy are interpreted as etch grooves caused by stacking faults in between split partial dislocations. It can be assumed that the sensitivity to chemical etching is attributed to an anisotropic surface energy of the fcc lattice. This assumption is supported by the fact that the effect is not equally pronounced in all grains as well as the different removal rates for certain grains and the strongly faceted surface topography that are observed after etching, Figure 1b, e. However, this does imply that the anisotropy of the surface energy is considerably higher in the present steel as compared to chrome-nickel austenitic stainless steels that only exhibit an anisotropy of approximately 10 % between (100) and (111) based on ab initio calculations [14].

The deformation mechanism in ambient air of steel X30MnCrN16-14 (grade 1.4678) was investigated in detail in [15, 16]. Upon plastic strain, the microstructure deformed by mechanical twinning as well as by planar dislocation slip, also known as TWinning Induced Plasticity (TWIP), *Figure 2*. Strain induced α'-martensite was not observed, as analysed by electron back scatter detection as well as by Feritscope in the necking area of the tensile specimens tested in air (this study), Figure 2. The measured stacking fault energy (SFE) of steel X30MnCrN16-14 is 22 mJ/m^2 [16]. This corresponds well with the calculated stacking fault energy map for iron-chrome-manganese-nitrogen austenitic steels [17]. A stacking fault energy of 18 mJ/m^2 is reported to be the threshold value below which austenite→ε-martensite or austenite→α'-martensite occurs whereas twinning is the predominant deformation mechanism for steels with stacking fault energys between 18 mJ/m^2 and 28 mJ/m^2 [17]. Stacking fault energy is a function of chemical composition. As mentioned before, local chemical composition varies, as identified by Lichtenegger-Bloech etching, Figure 1a. However, no α'-martensite was detected which means that the local deviations in chemical composition and thus stacking fault energy do not change the deformation mode.

Tensile tests were performed in both, air and H$_2$ atmosphere, *Table 2*, *Figure 3*. The yield strength (YS) is not affected by hydrogen. However, when tested in hydrogen, the specimen fails without noticeable necking and ultimate tensile strength (UTS), reduction of area (RA) and elongation at fracture (El) are strongly reduced. The relative reduction of area (RRA = RA$_{H2}$/RA$_{air}$) was 0.54 which was slightly higher compared to similar steels tested under identical conditions (RRA = 0.3 to 0.4) [10].

Fractographic investigations were performed on the specimens tested in air and H$_2$ atmosphere, *Fig-*

Table 2. Results of tensile tests in air (0.1 MPa, RT) and hydrogen (10 MPa, RT). The data in H$_2$ represent mean values of 3 repetitions.

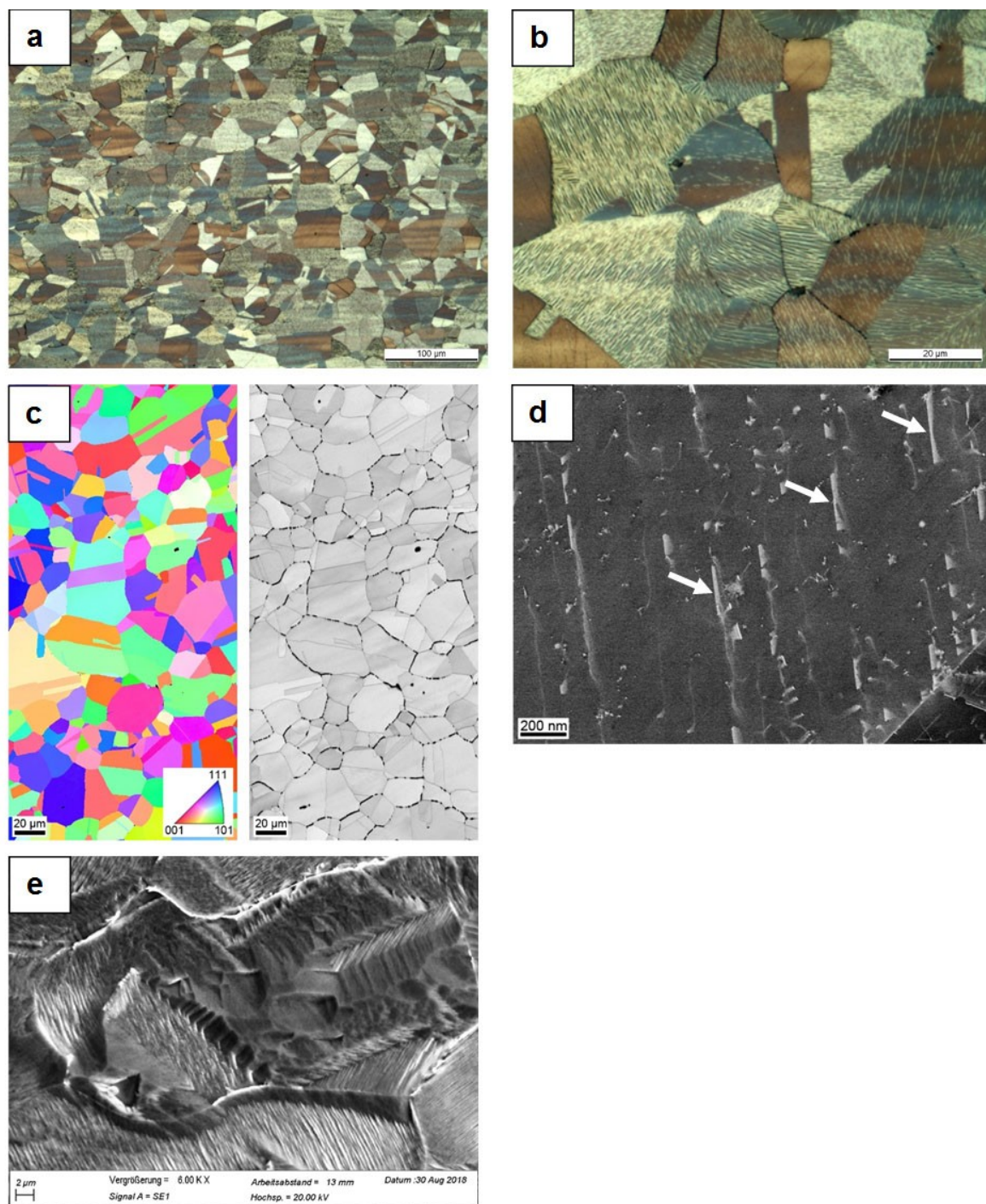| Test atmosphere	Yield strength	Ultimate tensile strength	Reduction of area	Elongation at fracture
	[MPa]	[MPa]	[%]	[%]
air	509	963	69.8	61.8
H$_2$	506	926	37.4	35.3

Figure 1. Cross section, microstructure in the as-delivered condition. a and b) Lichtenegger-Bloech etchant. c) inverse pole figure and image quality maps from electron back scatter detection. d) electron channeling contrast image showing stacking faults (white arrows). e) V2 A etchant, scanning electron microscopy image.

ures 4, 5. In air, the specimen failed by typical cup-cone fracture, Figure 4a. Micro voids as well as cracks were observed in the centre region and in the shear region. From a macroscopic viewpoint, the cracks appear to be aligned along the rolling texture of the plate semi finished product, Fig-
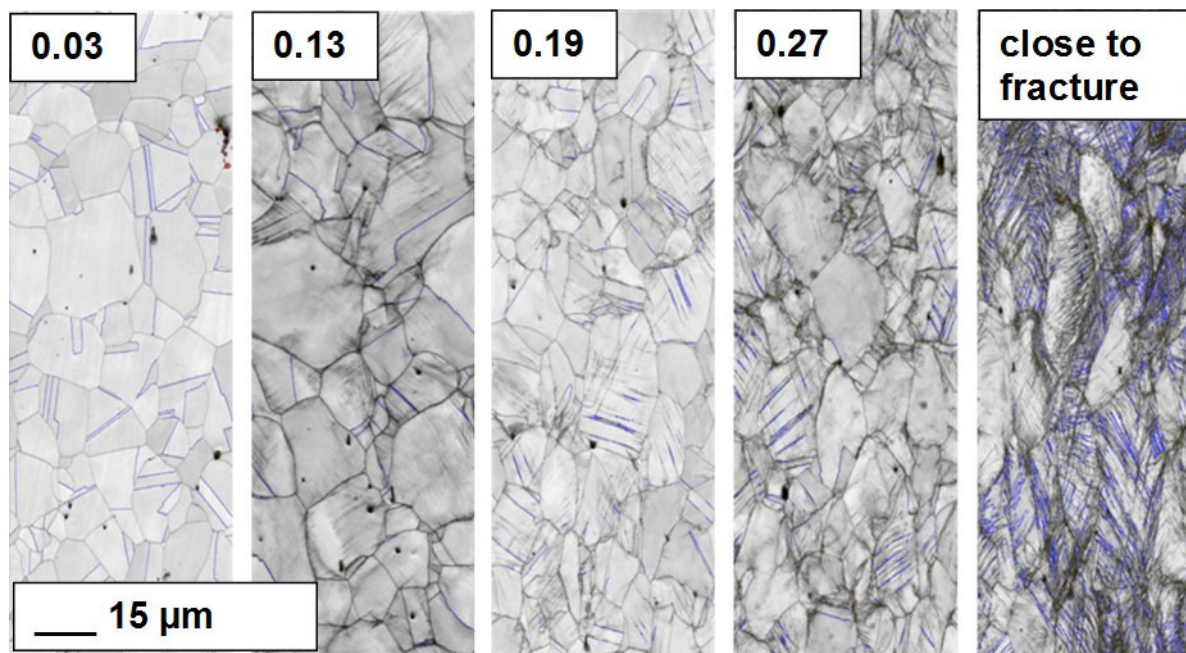
Figure 2. Deformation mechanism of steel X30MnCrN16-14. electron back scatter detection analysis at different engineering strains showing the evolution of twin formation (blue lines). Unpublished data from [15], reproduced with permission.
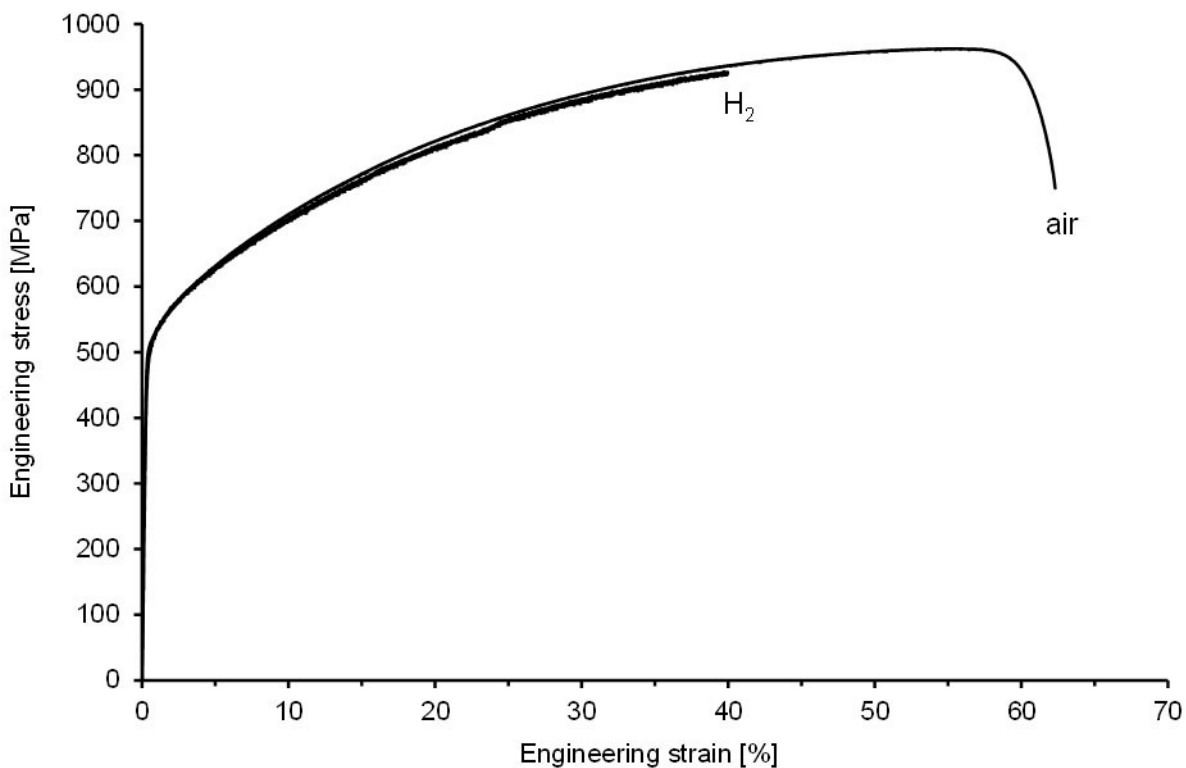

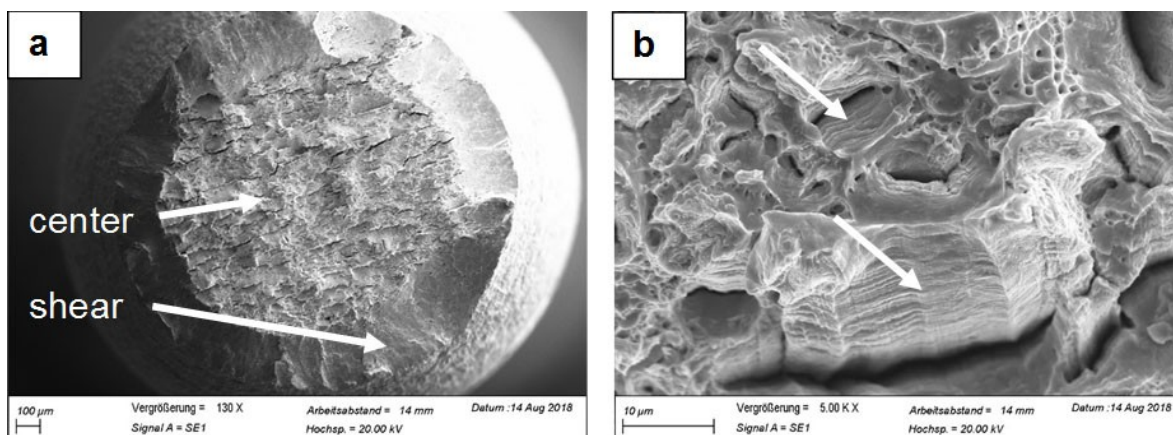**Figure 3.** Typical engineering stress-strain curves in air (0.1 MPa, RT) and H$_2$ (10 MPa, RT).

Figure 4. Tensile specimen tested in air (0.1 MPa, RT). a) Overview of the fracture surface. b) Detail from the centre region, the white arrows indicate facets with slip traces.
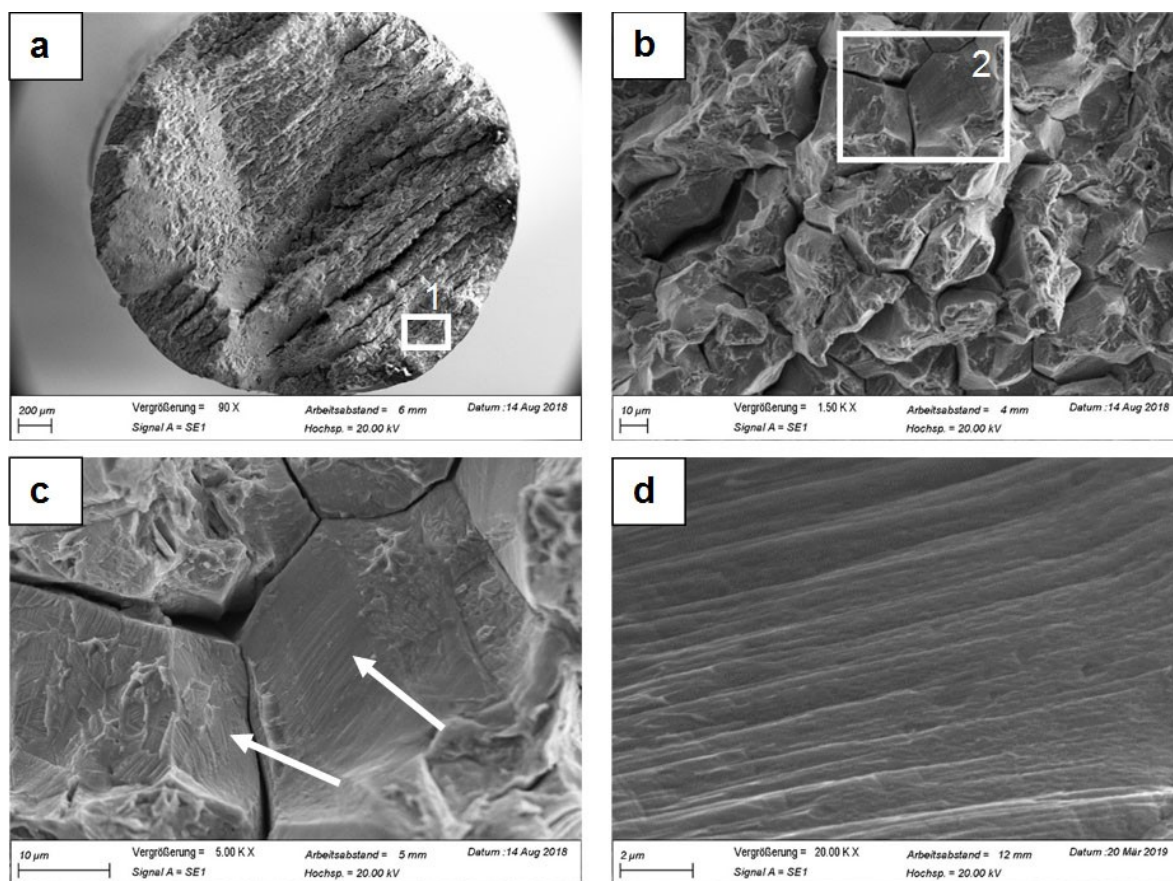

Figure 5. Tensile specimen tested in H_2 (10 MPa, RT). a) Overview of the fracture surface. b) Detail 1 showing predominantly intergranular fracture. c) Detail 2 showing slip traces on the facets. d) Higher magnification of slip traces on facets.

ure 4a. Slip traces were clearly visible on the facets of the open cracks, Figure 4b.

In hydrogen gas, the specimen failed without macroscopic necking. Macroscopic cracks were much larger compared to air and appear also to be aligned presumably along the sheet plane of the semi finished product, Figure 5a. The outer diameter of the fracture surface was characterized by a mixture of transgranular and boundary fracture. The size of the boundary facets corresponds with

the grain size implying predominantly intergranular fracture, Figure 5b. Fracture along twin boundaries was not investigated in detail and cannot be excluded. However, slip traces were clearly visible on the facets, Figure 5c, d. This fracture appearance is very similar to those reported for other austenitic manganese-nitrogen TWIP steels tested under similar conditions [9, 10].

In modern hydrogen embrittlement models like hydrogen enhanced localized plasticity (HELP), the effect of hydrogen on the mechanical properties of metals and alloys is explained by hydrogen-dislocation interactions [18]. In particular, there is growing evidence that hydrogen enhances the localization of deformation by energetically stabilizing the edge component of dislocations relative to the screw component [18–20]. For the given steel, the inherent plastic deformation is characterized by planar deformation modes, i.e. by planar dislocation motion and by mechanical twinning which is caused by planar glide of Shockley partial dislocations [17, 21]. That is, it appears that hydrogen amplifies and accelerates the inherent planar deformation modes. Dislocation pile up at twin or grain boundaries occurs much faster resulting in high stresses at such obstacles leading to twin or grain boundary separation with visible slip traces. In addition, hydrogen may lead to faster twin formation and dislocation pile up at the already formed twins resulting in premature failure. It is important to mention, that a highly twinned microstructure (twinning initiated prior to the exposure to hydrogen) shows little deterioration of tensile properties under the influence of hydrogen [22]. This implies that twinning under the influence of hydrogen is the predominant deteriorating mechanism in TWIP steels.

4 Summary

The microstructure of steel X30MnCrN16-14 was fully austenitic with parallel arrays of stacking faults inside the grains. The deformation was characterized by mechanical twinning and planar dislocation slide, as analysed in [15]. When tensile tested in hydrogen atmosphere at 10 MPa and room temperature, the elongation at fracture as well as the reduction of area was severely reduced compared to testing in air. Fractography of the speci-

men tested in H_2 revealed predominantly intergranular fracture with clearly visible slip traces on the facets. Correlating this with deformation modes reported in the open literature, it can fairly be assumed that the inherent planar deformation modes are facilitated by hydrogen resulting in premature failure which supports the hydrogen enhanced localized plasticity (HELP) theory.

Acknowledgements

5 References

[1] T. Michler, M. Lindner, U. Eberle, J. Meusinger, in R.P. Gangloff, B.P. Somerday (Eds.), *Gaseous hydrogen embrittlement of materials in energy technologies, vol. 1*, Woodhead, **2012**.

[2] S. Lindner, in Proc. 16. Int. Stuttgarter Symp.: Automobil- und Motorentechnik, Vol 2, Springer, **2016**, 55–64.

[3] P.J. Uggowitzer, R. Magdowiski, M.O. Speidel, *ISIJ Int.* **1996**, *36*, 901.

[4] J.C. Rawers, *J. Mater. Sci.* **2008**, *43*, 3618.

[5] M. Milititsky, D.K. Matlock, A. Regully, N. Dewispelaere, J. Penning, H. Hanninen, *Mat. Sci. Eng. A* **2008**, *496*, 189.

[6] S. Liu, D. Liu, S. Liu, *J. Mater. Sci.* **2007**, *42*, 7514.

[7] Z. Yuan, Q. Dai, X. Cheng, K. Chen, W. Xu, *Mater. Sci. Eng. A* **2008**, *475*, 202.

[8] H. Li, Z. Jiang, Z. Zhang, B. Xu, F. Liu, in Proc. Sino-Swedish Mat. Symp. **2007**: 330–334.

[9] T. Michler, J. Naumann, *Int. J. Hydrogen Energy* **2010**, *35*, 1485.

[10] T. Michler, C. San Marchi, J. Naumann, S. Weber, M. Martin, *Int. J. Hydrogen Energy* **2012**, *37*, 16231.

[11] B.L. Bramfitt, A.O. Benscoter, *Metallographer's Guide: Practice and Procedures for Irons and Steels*, ASM International, **2001**.

[12] P. Deimel, C. Hanisch, *Int. J. Hydrogen Energy* **1989**, *14*, 147.

[13] T. Michler, Y. Lee, R.P. Gangloff, J. Naumann, *Int. J. Hydrogen Energy* **2009**, *34*, 3201.

[14] H. Pitkänen, M. Alatalo, A. Puisto, M. Ropo, K. Kokko, L. Vitos, *Surf. Sci.* **2013**, *609*, 190.

[15] W. Bleck, Report of the Collaborative Research Center (SFB) 761 "Steel-ab initio", transfer project T1, **2015**, accessible via http://www.stahl-abinitio.de/sites/default/files/inline-files/Berichtsband_2015.pdf.

[16] J.E. Wittig, D.T. Pierce, L. Mosecker, A. Saeed-Akbari, M. Beigmohamadi, J. Mayer, *Microsc. Microanal.* **2013**, *19*, 1736.

[17] L. Mosecker, A. Saeed-Akbari, *Sci. Technol. Adv. Mater.* **2013**, *14*, 1.

[18] H.K. Birnbaum, P. Sofronis, *Mater. Sci. Eng. A* **1994**, *176*, 191.

[19] J.P. Chateau, D. Delafosse, T. Magnin, *Acta Mater.* **2002**, *50*, 1523.

[20] M.L. Martin, I.M. Robertson, P. Sofronis, *Acta Mater.* **2011**, *59*, 3680.

[21] S. Allain, J.-P. Chateau, D. Dahmoun, O. Bouaziz, *Mater Sci Eng A* **2004**, *38*, 272.

[22] Y.H. Fan, F. Cui, L. Lu, B. Zhang, *J. Alloys and Compounds* **2019**, *788*, 1066.